

The Multitude of Unresolved Continuum Sources at 1.6 microns in Hubble Space Telescope images of Seyfert Galaxies

A. C. Quillen¹, Colleen McDonald, A. Alonso-Herrero, Ariane Lee, Shanna Shaked, M. J. Rieke,
& G. H. Rieke,
Steward Observatory, The University of Arizona, Tucson, AZ 85721

ABSTRACT

We examine 112 Seyfert galaxies observed by the Hubble Space Telescope (HST) at $1.6\mu\text{m}$. We find that $\sim 50\%$ of the Seyfert 2.0 galaxies which are part of the Revised Shapeley-Ames (RSA) Catalog or the CfA redshift sample contain unresolved continuum sources at $1.6\mu\text{m}$. All but a couple of the Seyfert 1.0–1.9 galaxies display unresolved continuum sources. The unresolved sources have fluxes of order a mJy, near-infrared luminosities of order 10^{41} erg/s and absolute magnitudes $M_H \sim -16$. Comparison non-Seyfert galaxies from the RSA Catalog display significantly fewer ($\sim 20\%$), somewhat lower luminosity nuclear sources, which could be due to compact star clusters. We find that the luminosities of the unresolved Seyfert 1.0-1.9 sources at $1.6\mu\text{m}$ are correlated with $[\text{OIII}]5007\text{\AA}$ and hard X-ray luminosities, implying that these sources are non-stellar. Assuming a spectral energy distribution similar to that of a Seyfert 2 galaxy, we estimate that a few percent of local spiral galaxies contain black holes emitting as Seyferts at a moderate fraction, $\sim 10^{-1}$ – 10^{-4} , of their Eddington luminosities.

We find no strong correlation between $1.6\mu\text{m}$ fluxes and hard X-ray or $[\text{OIII}] 5007\text{\AA}$ fluxes for the pure Seyfert 2.0 galaxies. These galaxies also tend to have lower $1.6\mu\text{m}$ luminosities compared to the Seyfert 1.0-1.9 galaxies of similar $[\text{OIII}]$ luminosity. Either large extinctions ($A_V \sim 20 - 40$) are present towards their continuum emitting regions or some fraction of the unresolved sources at $1.6\mu\text{m}$ are compact star clusters. With increasing Seyfert type the fraction of unresolved sources detected at $1.6\mu\text{m}$ and the ratio of $1.6\mu\text{m}$ to $[\text{OIII}]$ fluxes tend to decrease. These trends are consistent with the unification model for Seyfert 1 and 2 galaxies.

Subject headings:

1. Introduction

Studies of active galactic nuclei (AGNs) have often focused on high luminosity objects since in these objects the active nucleus dominates the emission of the host galaxy. Study of the

¹aquillen@as.arizona.edu

lower luminosity objects is often hampered by confusion with emission from the galaxy in which the AGN resides (e.g., Edelson, Malkan & Rieke 1987; Spinoglio et al. 1995, Fadda et al. 1998; Alonso-Herrero, Ward & Kotilainen 1996). However, the high angular resolution of the Hubble Space Telescope (HST) allows us to probe the nuclei with a beam area about 30 times smaller than is typically achieved with ground-based observations at these wavelengths. This enables us to separate the nuclear emission from that of the surrounding galaxy with unprecedented accuracy. Malkan, Gorjian & Tam (1998) have carried out a survey of nearby Seyfert galaxies using WFPC2 on board HST at $0.6\mu\text{m}$. In this work, unresolved continuum sources (e.g., Malkan et al. 1998) were detected almost exclusively in Seyfert 1 galaxies. These authors postulated that extinction associated with a central torus (e.g., Antonucci 1993) or on larger scales makes it difficult to detect nuclear sources associated with Seyfert 2 galaxies.

Because extinction is comparatively reduced at longer wavelengths, the dusty torus model unifying Seyfert 1 and 2 galaxies suggests that we should detect nuclear emission from a larger fraction of Seyfert galaxies in the near-infrared than is possible at visible wavelengths. Near-infrared ground based studies have detected bright non-stellar unresolved nuclear sources in a few bright Seyfert 2 galaxies (e.g., Malkan & Filippenko 1983; Alonso-Herrero, Ward & Kotilainen 1996), implying that the extinction at this wavelength can be low enough for continuum radiation to escape the central region. Here we report on a survey of Seyfert galaxies observed with NICMOS (the Near Infrared Camera and Multi-Object Spectrograph) on board HST at $1.6\mu\text{m}$. By using NICMOS, we combine the high angular resolution of HST with the ability to carry out an imaging survey in the near-infrared.

2. Archival Observations

We compiled images from the HST archive that were observed with the F160W filter at $1.6\mu\text{m}$ with NICMOS. These galaxies were observed primarily as part of three observing programs which we identify by the proposal ID number used by the Space Telescope Science Institute. Galaxies from proposal 7330 were drawn from the Revised Shapely-Ames (RSA) Catalog ($B_T < 13.4$; Sandage & Tammann) and are described by Regan & Mulchaey (1999). This proposal includes a comparison sample of non-active galaxies matching in luminosity, Hubble type, color and redshift distribution to its Seyfert sample. Those from proposal 7328 are Seyfert galaxies with redshifts less than 0.019 from Veron-Cetty & Veron (1993). Those from proposal 7867 are the 23 Seyfert 1.8-2 galaxies from the CfA redshift survey (excluding NGC 1068 which was a GTO target) and are described by Martini & Pogge (1999). In total we find 35 Seyfert galaxies identified in the CfA redshift survey (e.g., Huchra & Burg 1992; Osterbrock & Martel 1993) including NGC 1068 and about 10 Seyfert 1.0-1.5 galaxies. A total of 26 galaxies were listed as Seyfert galaxies in the survey by Ho, Filippenko & Sargent (1995), and 57 galaxies are part of the extended RSA sample discussed by Maiolino & Rieke (1995). The galaxies are listed in Tables 1-5.

The CfA sample is drawn from the fraction of the sky defined either by $\delta \geq 0^\circ$ and $b \geq 40^\circ$ or

$\delta \geq -2^\circ.5$ and $b \leq -30^\circ$. Because it is not a color selected sample, it should be relatively free of selection effects that tend to enhance the proportion of galaxies with anomalously strong emission in the color used for selection (Huchra & Burg 1992; Osterbrock & Martel 1993). However, because many of the objects are moderately distant, the CfA sample does not sample the low luminosity tail of the Seyfert distribution (McLeod & Rieke 1995). It also does not contain enough Seyferts (only 51) to allow strong statistical tests. The RSA sample includes galaxies all over the sky. The primary selection criterion is that $B_T < 13.4$. The mean distance of this sample is $D = 34$ Mpc, about 3 times nearer than the CfA sample. Nuclear spectra are less contaminated by galaxy light and Seyferts at a larger range of galaxy inclinations and Hubble types are found in this sample (Maiolino & Rieke 1995). Unfortunately the spectroscopic identifications were not done with uniform data. The more uniform spectroscopic survey of Ho et al. (1995), also based on the RSA catalog but not covering the whole sky, has found a few additional low luminosity Seyfert galaxies which were not compiled by Maiolino & Rieke (1995). Ho et al. (1995) also discovered some broad line components not previously seen with lower quality spectra.

We group the Seyfert galaxies according to samples discussed in the literature. Table 1 contains all the galaxies which were part of the extended RSA sample (Maiolino & Rieke 1995). Subscripts are given to Seyferts which are also part of the CfA sample (e.g., Osterbrock & Martel 1993) or which were observed by Ho et al. (1995). Galaxies which were not listed by Maiolino & Rieke (1995) but are contained in the CfA sample are included in Table 2. Additional Seyferts are listed in Table 3. Non-Seyfert galaxies are listed in Tables 4 and 5.

Images were reduced with the ‘niced’ data reduction software (McLeod 1997) using on orbit darks and flats. Each set of images was then combined according to the position observed. The pixel size for the NICMOS camera 2 is $\sim 0''.076$ and for camera 1 is $\sim 0''.043$. The FWHM for an unresolved point source is $\sim 0''.13$ at $1.6\mu\text{m}$ with HST corresponding to ~ 20 pc for the mean galaxy at a distance of 33 Mpc in the RSA sample. Almost all of the images were observed with the sequence of non-destructive reads in the MULTIACCUM mode. We found no evidence for saturation in any of the images.

3. Unresolved nuclear sources

At the center of these galaxies we expect contribution from both an underlying stellar component and an unresolved nucleus. To measure the flux from the unresolved component we must subtract a resolved galaxian model. We opted to use exponential and power law galaxian profiles since Carollo, Stiavelli, & Mack (1998) find little or no morphological/photometric evidence for a smooth, $R^{1/4}$ law bulge in WFC2 images of galaxy bulges. Since we fit the galaxy profile to the central arcsecond only, a profile with more free parameters is not required.

For each camera we measured a point spread function from stars in the images. We constructed a library of galaxy profiles for different scale lengths, h , or exponents, α , by convolving

the point spread function with exponential profiles (surface brightness $\propto e^{-r/h}$) or powerlaw profiles (surface brightness $\propto r^{-\alpha}$). We then fit the sum of a convolved galaxian profile and the point spread function to the galaxy surface brightness profiles. When the exponential profile was fit we varied the central surface brightness, the scale length and the flux of an additional unresolved component. When the powerlaw profile was fit we varied the surface brightness at a radius of $1''$, the exponent, α , and the flux of an additional unresolved component. We also fit both powerlaw and exponential profiles without unresolved components to each galaxy. We then identified the best fitting profile shape. Sample fits to the galaxy surface brightness profiles are shown in Figure 1. For these galaxies we checked that the estimated unresolved flux was not strongly dependent upon the range of radius fit. Doubling the fitting radius affected the estimated nuclear flux by less than 1%. In NGC 5252 we also fit the profile out to a radius of $5''$ with a Nuker law profile (a double powerlaw as described by Faber et al. 1997) and measured a nuclear flux that was only 10% higher than that found with a single powerlaw profile and a fit within $1''$. Parameters describing the best fitting profiles are listed in Tables 1-4. The error of the flux from the unresolved component was estimated from the difference between the exponential and powerlaw profile fit. When the best fitting profile contained no unresolved component we then used the best fitting profile with an unresolved component to derive an upper limit on the flux of a possible additional unresolved source.

At $1.6\mu\text{m}$ an unresolved (point) source observed with NICMOS shows a prominent diffraction ring with a radius of $\sim 0''.3$. This is the dominant feature we fit in the surface brightness profiles. The error in this procedure we estimated from the scatter in the residuals and was about $\pm 10\%$ of the measured flux for the bright sources and about 50% for most of the fainter sources and is highest in the images with bright compact underlying surface brightness profiles. To test our fitting procedure we recovered fluxes at these levels of accuracy from model images created with the iraf routine ‘mkobject’. For galaxies with extremely steep surface brightness profiles the results of the fit are necessarily not unique. For $h \gtrsim 0''.1$ and $\alpha \lesssim 1.3$ no diffraction ring is seen clearly in the surface brightness profile of a model image after convolution with the point spread function. This describes the region in parameter space where the fitting procedure becomes uncertain. In other words, for steep galaxy profiles we cannot tell the difference between the sum of a point source and a exponential at $h \sim 0''.1$ and an exponential profile with a similar scale length.

We list in tables 1-4 a symbol describing the morphology of the central arcsecond. When the unresolved point source dominated the image we denoted in Tables 1-4 a type ‘*’. When the diffraction ring was faint but seen both visually in the image and in the surface brightness profile we denote ‘F’. When no diffraction ring was seen but the surface brightness profile was consistent with the sum of an unresolved nuclear component and a smoother resolved exponential profile we denote ‘:’. When the nuclear profile was resolved we denote ‘-’.

The flux of the nuclear source was corrected using aperture corrections derived from a point spread function which we generated with Tinytim (Krist et al. 1998). To convert fluxes into Jy we used conversion factors 2.360×10^{-6} , 2.190×10^{-6} , 2.776×10^{-6} Jy per DN/s for Cameras 1, 2

and 3 respectively. This flux calibration is based on measurements of the standard stars P330-E and P172-D during the Servicing Mission Observatory Verification program and subsequent observations (M. Rieke 1999, private communication).

3.1. The fraction of galaxies with unresolved emission

In Table 6 we compile the fraction of various Seyfert type galaxies which display unresolved nuclear sources. All but one (NGC 4594) of the Seyfert 1.0-1.9 galaxies (types listed by Maiolino & Rieke 1995 and Osterbrock & Martel 1993) displayed an unresolved nuclear source. Additionally two galaxies listed as S1.9’s by Ho et al. 1995 (NGC 2639 and NGC 4258) did not display unresolved emission. About 50% of the Seyfert 2.0 galaxies displayed unresolved sources. The CfA and Ho samples have the lowest fraction of unresolved nuclear sources among the Seyfert 2.0 galaxies possibly because they are the most uniform in spectral quality and Seyfert typing compared to the other samples. The presence of weak broad line emission may indicate that continuum radiation at $1.6\mu\text{m}$ can escape the central pc.

About 50% of the Seyfert 2 galaxies from proposal 7330 displayed significant unresolved emission compared to 24% of the control or non-Seyfert galaxies drawn from this same proposal. The fraction of galaxies with more robustly identified unresolved sources (those labelled ‘*’ and ‘F’) is also larger in the Seyfert sample than the non-Seyfert sample. Though our fitting routine is not unique, particularly when the galaxy surface brightness profiles are steep, if we exclude the more marginal cases, we still find that the Seyfert and non-Seyfert samples differ. This implies that the Seyfert galaxies are more likely to display unresolved nuclear sources at $1.6\mu\text{m}$ than the non-Seyfert galaxies. There must be an intrinsic difference between galaxies identified as Seyferts and those not identified as Seyferts in the RSA Catalog.

HST observations of nearby spiral galaxies have found that many harbor nuclear star clusters, a small fraction of which ($\sim 5\%$) are unresolved (Carollo et al. 1997). The non-Seyfert galaxies studied by Carollo et al. (1997) are somewhat closer than the galaxies in our sample, lying at a mean distance of 23 Mpc, compared to 34 Mpc, the average distance of our RSA sample. Using a color $V - H \sim 2.65$, the star clusters from Carollo et al. (1997) have fluxes ranging from 0.01 to 5 mJy, making them similar in magnitude to the unresolved fluxes we have measured in the Seyfert sample. Placing these galaxies at distances similar to our Seyfert galaxies would result in a somewhat larger number of the sources being unresolved, however, it would also decrease their brightness.

We can also compare the luminosity distributions of the unresolved nuclear sources between the non-Seyfert and Seyfert RSA samples (galaxies observed as part of proposal 7330). We estimate the luminosity at $1.6\mu\text{m}$ by $\nu f_\nu * 4\pi D^2$ for a distance of D . We used distances from the Nearby Galaxies Catalog (Tully 1988) or from the radial velocity with a Hubble constant of $75 \text{ km s}^{-1} \text{ Mpc}^{-1}$.

We find that the luminosity distribution of unresolved sources in proposal 7330 and the RSA sample differ, even though their redshift distributions are similar (see Figure 2). The non-Seyfert unresolved sources tend to have lower luminosities. We conclude that the luminosities and fraction of unresolved nuclear sources in Seyferts galaxies differ from those found in non-Seyfert galaxies.

3.2. Comparison with hard X-ray and [OIII]5007Å

Mid-infrared photometric and optical and UV spectroscopic surveys have found that Seyfert 2 galaxies are more likely to harbor nuclear star formation (Gonzalez-Delgado & Perez 1993; Maiolino et al. 1995); This might suggest that a galaxy identified as a Seyfert 2 galaxy may be more likely to harbor a brighter compact star cluster than a non-Seyfert galaxy. In this case the unresolved sources in the Seyfert 2 galaxies could be due to compact star clusters rather than non-stellar AGN emission.

There are a couple of ways to test this hypothesis. One way is to search for variability in multi-epoch observations. Quillen et al. (2000) found that 8/13 of the unresolved sources in Seyfert 1.8 and 1.9 galaxies varied, proving that they are non-stellar, associated with the central pc of an AGN, and not emission from bright nuclear stellar clusters. However the $1.6\mu\text{m}$ unresolved emission in Seyfert 2.0 galaxies lacking any broad line component could still arise from compact star clusters. Another way to test this hypothesis is by searching for correlations between the $1.6\mu\text{m}$ emission, and [OIII] or hard X-ray emission. Previous studies have shown that [OIII] and hard X-ray luminosities are correlated with AGN activity (Mulchaey et al. 1994; Keel et al. 1994, Bassani et al. 1999), and that the near infrared flux is correlated with hard X-ray and [OIII] luminosity in bright Seyferts (Alonso-Herrero, Ward & Kotilainen 1996; Alonso-Herrero et al. 1997). In Figure 3 we compare luminosities computed at $1.6\mu\text{m}$ with those estimated with [OIII]5007Å and hard X-ray fluxes. [OIII]5007Å fluxes were taken from Ho et al. (1995), Whittle (1992), Bassani et al. (1999) and Risaliti et al. (1999) and whenever possible are corrected for reddening using the Balmer decrement. Hard X-ray fluxes (2-10keV) were taken from the compilations of Bassani et al. (1999), Risaliti et al. (1999), and Mulchaey et al. (1994) and were corrected for observed absorption when the sources were not Compton thick. As discussed in these compilations the fluxes have been measured with a variety of different instruments, apertures and calibration techniques. Some of the scatter in these plots may be due to inconsistencies between the comparative measurements of the [OIII] or hard X-ray fluxes.

We computed Spearman rank-order correlation coefficients on the fluxes for the Seyferts shown in Figure 3 (see Table 7). There is a convincing correlation between [OIII] and $1.6\mu\text{m}$ fluxes and between hard X-ray and $1.6\mu\text{m}$ fluxes in the Seyfert 1.0-1.9 galaxies. However, only a weak correlation is seen in the pure Seyfert 2.0 galaxies. This lack of a strong correlation suggests that extremely large extinctions are present towards the Seyfert 2.0 nuclei. Alternatively some fraction of the unresolved $1.6\mu\text{m}$ Seyfert 2.0 sources could be due to star clusters.

Starburst galaxies are emitters of hard X-rays which could be arising from hidden AGN, high mass X-ray binaries, or inverse Compton scattering from high energy particles associated with supernovae (e.g., Ohashi & Tsuru 1992). For comparison to our galaxy nuclei, we estimate the $1.6\mu\text{m}$ to hard X-ray luminosity ratio for the infrared luminous starburst galaxy NGC 3256. NGC 3256 has a hard X-ray (2-10 keV) luminosity of 2×10^{41} erg/s (Moran, Lehnert, & Helfand 1999) and a luminosity at $1.6\mu\text{m}$ of 3.4×10^{43} erg/s which we estimate based upon the H band aperture photometry of Glass (1973). The ratio of the $1.6\mu\text{m}$ to hard X-ray luminosity is 170 (a log of 2.2) which is above the Seyfert 2 points shown in Fig. 3b. The bulk of the hard X-ray emission in the Seyfert 2s must come from an AGN rather than a nuclear star cluster. If the hard X-ray emission came from a starburst then we would have expected even larger levels of soft X-ray emission which is generally not seen in Seyfert 2 galaxies (e.g., Mulchaey et al. 1994).

We see in Figure 3 that for a given [OIII] luminosity the Seyfert 1.8-1.9 galaxies have $1.6\mu\text{m}$ luminosities similar to or slightly lower than the Seyfert 1.0–1.5 galaxies. The Seyfert 2.0 galaxies, however, have lower $1.6\mu\text{m}$ fluxes. If the $1.6\mu\text{m}$ emission is associated with AGNs then there could be significant extinction, $A_V \sim 40$, towards the continuum emission region in the Seyfert 2 galaxies. A similar trend was observed in a smaller ground based sample by Alonso-Herrero, Ward & Kotilainen (1997). If the [OIII] luminosity is a reliable luminosity indicator, then Seyfert 2 galaxies have significantly larger extinctions towards their continuum emission regions than Seyfert 1.0–1.9 galaxies. The Seyfert 1.8–1.9 galaxies appear to be intermediate, suggesting that a partial view of the broad line region occurs when there is reduced extinction towards the near-infrared continuum emission region.

The star formation models of Fioc & Rocca-Volmerange (1997) predict that a 10^6 year old solar metallicity instantaneous starburst should have a ratio of [OIII] to $1.6\mu\text{m}$ luminosity of 2.7. For older starbursts the [OIII] luminosity drops rapidly compared to the $1.6\mu\text{m}$ luminosity (at 10^7 years the ratio is ~ 0.002). The emission line ratios of these galaxy nuclei have caused them to be identified as Seyferts, so it is unlikely that most of the [OIII] emission arises from a starburst (though starburst models for Seyfert line ratios have been proposed; Terlevich & Melnick 1985). However, we can consider what minimum starcluster ages could be consistent with a [OIII] contribution from the starburst contribution that does not dominate the emission line spectrum.

The [OIII] luminosities of the Seyfert 1.0-1.9 galaxies are well above that predicted from a young starburst. However the [OIII] to $1.6\mu\text{m}$ luminosity ratios of the Seyfert 2 galaxies are similar to those observed in 10^6 year old starbursts. It is unlikely that the $1.6\mu\text{m}$ emission in the Sy 2 galaxies is associated with a 10^6 year old starcluster, because then the nuclear spectrum would be that of an HII region rather than a Seyfert. However older few million year old starclusters cannot be excluded. In this case the $1.6\mu\text{m}$ emission could be stellar and the narrow emissions lines associated with the AGN.

3.3. Minimum foreground extinctions

The spectral energy distribution of an old stellar population peaks at about $1.6\mu\text{m}$. If the spectral energy distribution of a continuum source associated with an AGN is similar to that of a quasar, which generally has a dip at $1.6\mu\text{m}$, then it should be the *most* difficult to detect against the background galaxy at this wavelength. Likewise Seyfert 1 galaxies have continua which are bluer than an old stellar population so we might expect that Seyfert 1 galaxies would be more difficult to detect at $1.6\mu\text{m}$ than in the visible bands. The “unification” model postulates that Seyfert 1 and 2 galaxies differ in terms of orientation angle (Antonucci 1993), and that a dusty torus absorbs a significant fraction of the optical/UV/X-ray luminosity. This implies that significant extinction in front of the nucleus may be present in Seyfert 2 galaxies. This extinction may account for the large number of unresolved point sources detected at $1.6\mu\text{m}$ compared to the non-detections reported by Malkan et al. (1998) at $0.606\mu\text{m}$.

The galaxies chosen by Malkan et al. (1998) for WFPC2 observations were galaxies from the Catalog of Quasars and Active Nuclei (Veron-Cetty & Veron 1993) with redshift less than 0.035. Galaxies observed with NICMOS as part of proposal 7328 were also chosen from this catalog, (restricted to $z < 0.019$), however most of the galaxies observed with NICMOS were not. Of the galaxies which were part of the 7328 proposal we detected unresolved emission from all Sy 1-1.9s (12 Sy 1.0-1.5s and 4 Sy 1.8,1.9s). Out of 13 Sy 2 galaxies, unresolved emission was detected from 8 at high confidence and from 1 with lower confidence. This fraction of Sy 1.8-2.0 with unresolved nuclear emission is larger than that reported by Malkan et al. (1998). Unfortunately, some of the WFPC2 images of this survey were saturated near the galaxy nuclei. Images observed with shorter exposure times might have displayed a larger number of unresolved nuclear sources.

We can assume that the level of stellar emission limits our ability to detect the non-stellar emission. An old stellar population commonly found in the central region of a galaxy has $V - H \sim 3.0$ (Frogel 1985). If Seyfert 2 galaxies are similar to Seyfert 1 galaxies in their inner regions then we can model the underlying emission as that of a Seyfert 1 with $V - H \sim 2.6$ (Alloin et al. 1995). For the non-stellar source to be detectable at $1.6\mu\text{m}$ (roughly H band) and undetectable at $0.6\mu\text{m}$ (roughly V band), the source must be redder than the stellar background. If we assume that foreground extinction is responsible for the redenning then the change in color must be larger than the difference between the nucleus and stellar color ($\Delta(V - H) \gtrsim 0.4$). Using $A_H \sim 0.176A_V$ (from Mathis 1990) $\Delta(V - H) \sim A_V - A_H \sim 0.824A_V$ which implies that foreground extinction at least $A_V \gtrsim 0.5$ is needed for the unresolved sources to be detectable at $1.6\mu\text{m}$ and not at $0.6\mu\text{m}$ against the stellar background. Some of the unresolved sources listed in Tables 1-3 are up to 100 times above the detection limit at $1.6\mu\text{m}$ (e.g., NGC 1068) which implies that extinctions of at least $A_V \gtrsim 5$ are required to account for their brightness at $1.6\mu\text{m}$ and faintness at visible wavelengths which would be consistent with a reduced detection rate in the optical survey (Malkan et al. 1998).

4. Summary and Discussion

We report on the discovery of a large number of unresolved continuum emission sources at $1.6\mu\text{m}$ in a significant fraction of nearby Seyfert galaxies observed with HST. Of the Seyfert 2 galaxies in the RSA and CfA samples 50–70% display unresolved continuum sources. For Seyfert 2.0 galaxies listed in Ho et al. (1995) only 10–35% of the Seyfert 2.0 galaxies displayed unresolved sources. All but 1 of the Seyfert 1.0-1.9 galaxies display unresolved sources. A comparison galaxy sample drawn from the RSA Catalog lacking Seyfert nuclei display significantly fewer ($\sim 20\%$) unresolved sources than Seyferts found in this catalog. We find that the luminosities and fraction of unresolved nuclear sources in Seyfert galaxies differ from those found in non-Seyfert galaxies.

The luminosities at $1.6\mu\text{m}$ are correlated with hard X-ray and [OIII] 5007\AA luminosities for the Seyfert 1.0-1.9 galaxies. These unresolved sources are therefore most likely non-stellar and not due to compact nuclear star clusters. The presence of weak broad line emission (in Seyfert 1.8 and 1.9 galaxies) appears to be coincident with the presence of a detectable unresolved continuum source at $1.6\mu\text{m}$. This is surprising since the size of the broad line region is expected to be much smaller than that containing the hot dust giving rise to the near-infrared emission (e.g., Barvainis 1987; Pier & Krolik 1993; Marconi et al. 2000). A partial covering of the broad line region may be directly associated with reduced extinction towards the near-infrared continuum emitting region. The near-infrared continuum emission region could be closer to the broad line region than previously considered.

We find no strong correlation between $1.6\mu\text{m}$ fluxes and hard X-ray or [OIII] 5007\AA fluxes for the pure Seyfert 2.0. These galaxies also tend to have lower $1.6\mu\text{m}$ luminosities compared to the Seyfert 1.0-1.9 galaxies of similar [OIII] luminosity. Either large extinctions ($A_V \sim 20 - 40$) are present towards their continuum emitting regions or/and some fraction of the unresolved sources at $1.6\mu\text{m}$ are compact star clusters. With increasing Seyfert type the fraction of unresolved sources detected at $1.6\mu\text{m}$ and the ratio of $1.6\mu\text{m}$ to [OIII] fluxes tend to decrease. These trends are consistent with the unification model for Seyfert 1 and 2 galaxies.

Assuming a color typical of a Seyfert 1 galaxy, only a moderate amount of foreground extinction, $A_V \gtrsim 0.5$, is required to account for the detections at $1.6\mu\text{m}$ and non-detections at $0.6\mu\text{m}$ (reported by Malkan et al. 1998) of the Seyfert 1.8-2.0 galaxies. We suspect that an even larger number of galaxies would display unresolved sources at longer wavelengths if observed at a similar angular resolution.

Accretion models for AGNs rely on two fundamental parameters to describe them, the black hole mass and the bolometric luminosity emitted, which we expect is dependent upon the accretion rate. Black hole masses have recently been measured with a variety of techniques (e.g., Richstone et al. 1998), however estimates of the bolometric luminosity exist for only a few nearby sources. We can crudely estimate the bolometric luminosity from that at $1.6\mu\text{m}$ by assuming a ratio of ~ 10 between the $1.6\mu\text{m}$ and mid-IR luminosity similar to that of Seyfert 2 galaxies (e.g, Fadda et al. 1998 and a ratio of ~ 10 between the mid-IR and bolometric luminosity (e.g., Spinoglio et

al. 1995). In units of the Eddington luminosity

$$\frac{L_{bol}}{L_{ED}} \sim 10^{-2} \left(\frac{L_{1.6\mu\text{m}}}{10^{41} \text{ergs/s}} \right) \left(\frac{L_{bol}/L_{1.6\mu\text{m}}}{100} \right) \left(\frac{M_{BH}}{10^7 M_{\odot}} \right)^{-1} \quad (1)$$

About 10% of the RSA sample of galaxies contains Seyfert nuclei with Seyfert 1.8-2 galaxies being 3 times more common than Seyfert 1-1.5 galaxies (Maiolino & Rieke 1995). Our RSA subsample contains a substantial fraction of Seyfert galaxies with $1.6\mu\text{m}$ luminosities of order 10^{41} ergs/s (see Figure 2). Since most of the galaxies are spiral galaxies we expect black hole masses in the range of $10^6 - 10^8 M_{\odot}$ (e.g., Richstone et al. 1998). The above estimate implies that the bolometric luminosities in Eddington units span the range $10^{-1} - 10^{-4}$ for black holes likely to reside in these galaxies. This range is consistent with previous estimates (e.g., Wandel 1991; Cavaliere & Padovani 1989), and suggests that a few percent of the black holes resident in local spiral galaxies are emitting as Seyferts at a moderate fraction of their Eddington luminosity. Longer wavelength observations will yield better estimates for the bolometric luminosities of these numerous low luminosity AGNs.

The Seyfert samples we have considered in this paper consist of Seyfert galaxies with clear optical spectroscopic identifications. A sample of active galaxies chosen in the mid-infrared (e.g. 10-50 microns) or with hard X-rays may yield a population of more highly obscured AGNs which may be much harder to detect both optically and at $1.6\mu\text{m}$.

Support for this work was provided by NASA through grant number GO-07869.01-96A from the Space Telescope Institute, which is operated by the Association of Universities for Research in Astronomy, Incorporated, under NASA contract NAS5-26555. We also acknowledge support from NASA project NAG-53359 and NAG-53042 and from JPL Contract No. 961633. This research has made use of the NASA/IPAC Extragalactic Database (NED) which is operated by the Jet Propulsion Laboratory, California Institute of Technology, under contract with the National Aeronautics and Space Administration. We thank M. Salvati, and K. Gordon for helpful discussions.

REFERENCES

- Alloin, D., Santos-Lleò, M., Peterson, B. M., Wamsteker, W., Altieri, B., Brinkmann, W., Clavel, J., Crenshaw, D. M., George, I. M., Glass, I. S., Johnson, W. N., Kriss, G. A., Malkan, M. A., Polidan, R. S., Reichert, G. A., Rodriguez-Pascual, P. M., Romanishin, W., Starr, C. H., Stirpe, G. M., Taylor, M., Turner, T. J., Vega, H., Winge, C., & Wood, D. O. S. 1995, *A&A*, 293, 293
- Alonso-Herrero, A., Ward, M. J., & Kotilainen, J. K. 1996, *MNRAS*, 273, 902
- Alonso-Herrero, A., Ward, M. J., & Kotilainen, J. K. 1997, *MNRAS*, 288, 977
- Antonucci, R. R. J. 1993, *ARA&A*, 31, 473
- Bassani, L., Dadina, M., Maiolino, R., Salvati, M., Risaliti, G., Della Ceca, R., Matt, G., & Zamorani, G. 1999, *ApJS*, 121, 473
- Barvainis, R. 1987, *ApJ*, 320, 537
- Carollo, C. M., Stiavelli, M., & Mack, J. 1998, *AJ*, 116, 68
- Carollo, C. M., Stiavelli, M., de Zeeuw, P. T., & Mack, J. 1997, *AJ*, 114, 2366
- Cavaliere, A., & Padovani, P. 1989, *ApJ*, 340, L5 Eddington recurrent activity
- Edelson, R. A., Malkan, M. A., & Rieke, G. H. 1987, *ApJ*, 321, 233
- Faber, S., Tremaine, S., Ajhar, E. A., Dressler, A., Gebhardt, K., Grillmair, C., Kormendy, J., Lauer, T. R., & Richstone, D. 1997, *AJ*, 114, 1771
- Fadda, D., Giuricin, G., Granato, G. L., & Vecchies, D. 1998, *ApJ*, 496, 117
- Fioc, M., & Rocca-Volmerange, B. 1997, *A&A*, 326, 950
- Frogel, J. A. 1985, *ApJ*, 298, 528
- Glass, I. S. 1973, *MNRAS*, 164, 155
- Gonzalez-Delgado, R. M., & Perez, E. 1993, *Ap&SS*, 205, 127
- Heckman, T. M. 1995, *ApJ*, 446, 101
- Ho, L. C., Filippenko, A. V., & Sargent, W. L. W. 1995, *ApJS*, 98, 477
- Huchra, J., & Burg, R. 1992, *ApJ*, 393, 90
- Keel, W. C., de Grijp, M. H. K., Miley, G. K., & Zheng, W. 1994, *A&A*, 283, 79
- Krist, J. E., Golimowski, D. A., Schroeder, D. J., & Henry, T. J. 1998, *PASP*, 110, 1046

- Maiolino, R., & Rieke, G. H. 1995, *ApJ*, 454, 95
- Maiolino, R., Ruiz, M., Rieke, G. H., & Keller, L. D. 1995, *ApJ*, 446, 561
- Malkan, M. A., Gorjian, V., & Tam, R. 1998, *ApJS*, 117, 25
- Malkan, M. A., & Filippenko, A. V. 1983, *ApJ*, 275, 477
- Marconi, A., Schreier, E. J., Koekemoer, A., Capetti, A. Axon, D., Macchetto, D., Caon, N. 2000, *ApJ*, 528, 276
- Martini, P., & Pogge, R. W. 1999, *AJ*, 118, 2646
- Mathis, J. S. 1990, *ARA&A*, 28, 37
- McLeod, K., & Rieke, G. H. 1995, *ApJ*, 441, 96
- McLeod, B. 1997, proceedings of the 1997 HST Calibration Workshop, eds. S. Casertano, R. Jedrzejewski, T. Keyes, and M. Stevens, published by the Space Telescope Science Institute, Baltimore, MD, p. 281
- Moran, E. C., Lehnert, M. D., & Helfand, D. J. 1999, *ApJ*, 526, 649
- Mulchaey, J. S., Koratkar, A., Ward M. J., Wilson, A. S., Whittle, M., Antonucci, R. R. J., Kinney, A. L., & Hurt, T. 1994, *ApJ*, 436, 586
- Ohashi, T., & Tsuru, T. 1992, in *Frontiers of X-Ray Astronomy* (Tokyo: Universal Academy Press), 435
- Osterbrock, D. E. & Martel, A. 1993, *ApJ*, 414, 552
- Pier, E. A., & Krolik, J. H. 1993, *ApJ*, 418, 673
- Quillen, A. C., Shaked, S., Alonso-Herrero, A., McDonald, C., Lee, A., Rieke, M. J., & Rieke, G. H. 2000, *ApJ*, 532, L17
- Regan, M. W., & Mulchaey, J. S. 1999, *AJ*, 117, 2676
- Richstone, D., Ajhar, E. A., Bender, R., Bower, G., Dressler, A., Faber, S. M., Filippenko, A. V., Gebhardt, K., Green, R., Ho, L. C., Kormendy, J., Lauer, T., Magorrian, J., & Tremaine, S. 1998, *Nature* 395A, 14
- Risaliti, G., Maiolino, R., & Salvati, M. 1999, *ApJ*, 522, 157
- Sandage, A., & Tammann, G. A. 1987, *A revised Shapley-Ames Catalog of bright galaxies*, (Carnegie Inst. of Washington Publ. 635, Washington DC)
- Spinoglio, L., Malkan, M. A., Rush, B., Carrasco, L., & Recillas-Cruz, E. 1995, *ApJ*, 453, 616

Terlevich, R., & Melnick, J. 1985, MNRAS, 213, 841

Tully, R. B. 1988, Nearby Galaxies Catalog, Cambridge University Press, Cambridge

Veron-Cetty, M.-P., & Veron, P. 1993, ESO Sci. Rep., 13, 1

Wandel, A. 1991, A&A, 241, 5

Whittle, M. 1992, ApJS, 79, 49

Fig. 1.— Examples of fits done to the galaxy surface brightness profiles to allow measurement of unresolved sources. The upper solid line is the galaxy profile and the upper dotted line is the resulting fit to this profile. The fit is a sum of a point source (shown as the dashed line) and an exponential profile or powerlaw profile which has been convolved with the point spread function (shown as the lower dotted line). The lower dot dashed line is the galaxy profile subtracted by the point source. The point spread functions shown were measured from stars observed in the same filter and with similar exposure times. a) NGC 5252 was observed with NICMOS Camera 2. Its profile is fit with an exponential galaxian profile. b) NGC 5252 profile fit with a powerlaw galaxian profile. c) UGC 12138 was observed with NICMOS Camera 1 and fit with an exponential galaxian profile. d) UGC 12138 fit with a powerlaw galaxian profile.

Fig. 2.— a) Luminosity distribution for the Seyferts with unresolved sources. The histogram filled with solid lines shows all the Seyferts listed in Tables 1-3, and the histogram filled with dotted lines corresponds to the Seyfert 2.0 galaxies. The histogram filled with dashed horizontal lines corresponds to the unresolved sources in the non-Seyfert, control galaxies. Absolute H magnitudes are shown on the top of the histograms. b) Luminosity distribution for the Seyferts in the RSA sample. c) Distance distribution for the total Seyfert, the RSA Seyfert and non-Seyfert samples. The distance distribution of the non-Seyfert galaxies matches that of the RSA sample.

Fig. 3.— a) Correlation between $1.6\mu\text{m}$ and $[\text{OIII}]5007\text{\AA}$ luminosities for the Seyferts listed in Tables 1-3. Upper limits are given when no nuclear point source was detected at $1.6\mu\text{m}$. Seyfert 2.0 galaxies appear to have weaker $1.6\mu\text{m}$ luminosities compared to Seyfert 1.9-1.0 galaxies. The correlation between $[\text{OIII}]$ and $1.6\mu\text{m}$ luminosity suggests that the majority of the unresolved sources are non-stellar. $[\text{OIII}]5007\text{\AA}$ fluxes were taken from Ho et al. (1995), Whittle (1992), Bassani et al. (1999) and Risaliti et al. (1999) and whenever possible are corrected for reddenning using the Balmer decrement. Points or upper limits are shown only when we found $[\text{OIII}]$ fluxes in these compilations. b) Correlation between $1.6\mu\text{m}$ and hard X-ray luminosities. Hard X-ray fluxes (2-10keV) were taken from Bassani et al. (1999), Risaliti et al. (2000) and Mulchaey et al. (1994) and were corrected for observed absorption, though some of the Seyfert 2.0 galaxies are Compton thick and so the fluxes do not represent the true X-ray luminosities. Points or upper limits are shown only when we found hard X-ray fluxes in these studies.

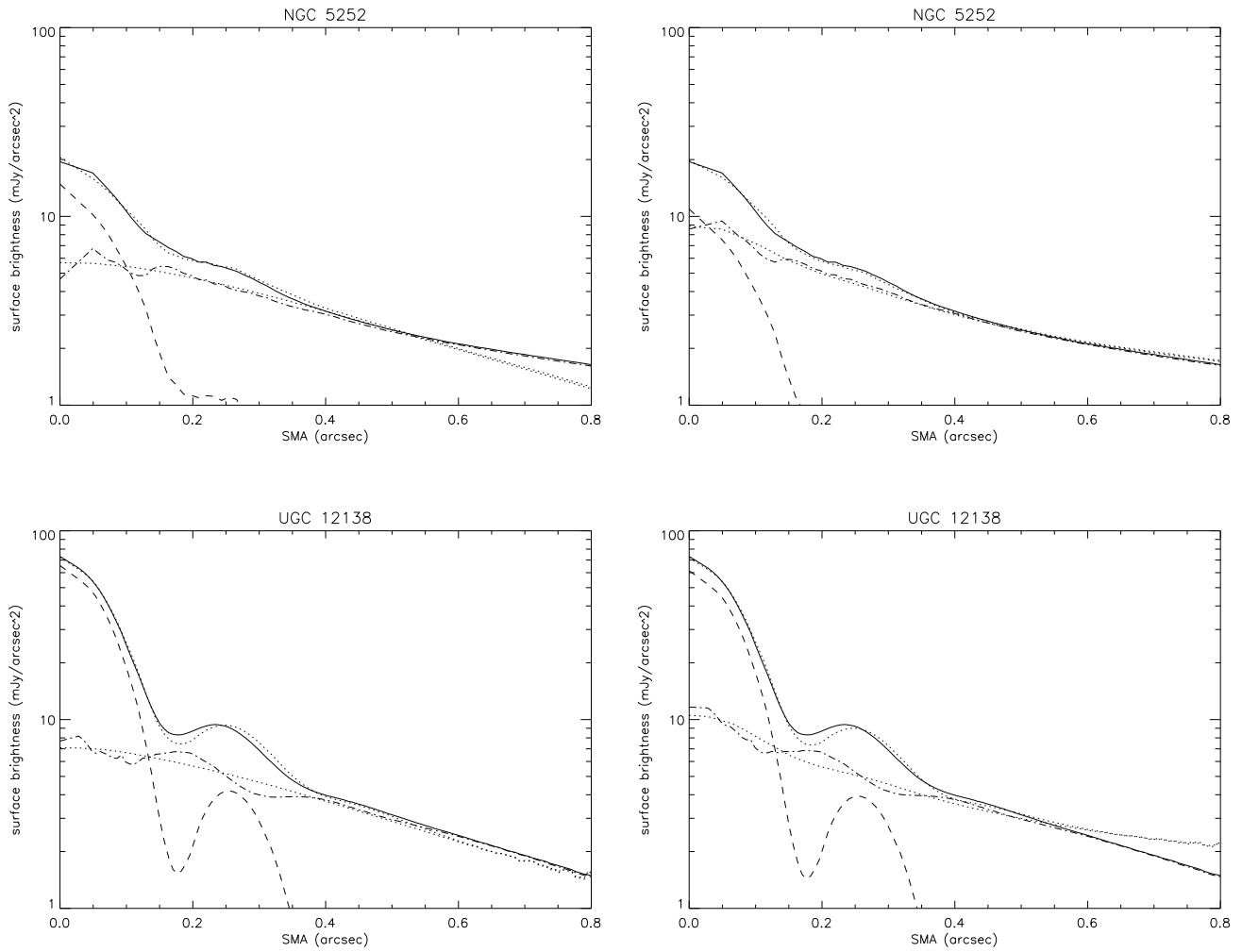


Fig. 1.— Examples of fits done to the galaxy surface brightness profiles to allow measurement of unresolved sources. The upper solid line is the galaxy profile and the upper dotted line is the resulting fit to this profile. The fit is a sum of a point source (shown as the dashed line) and an exponential profile or powerlaw profile which has been convolved with the point spread function (shown as the lower dotted line). The lower dot dashed line is the galaxy profile subtracted by the point source. The point spread functions shown were measured from stars observed in the same filter and with similar exposure times. a) NGC 5252 was observed with NICMOS Camera 2. Its profile is fit with an exponential galaxian profile. b) NGC 5252 profile fit with a powerlaw galaxian profile. c) UGC 12138 was observed with NICMOS Camera 1 and fit with an exponential galaxian profile. d) UGC 12138 fit with a powerlaw galaxian profile.

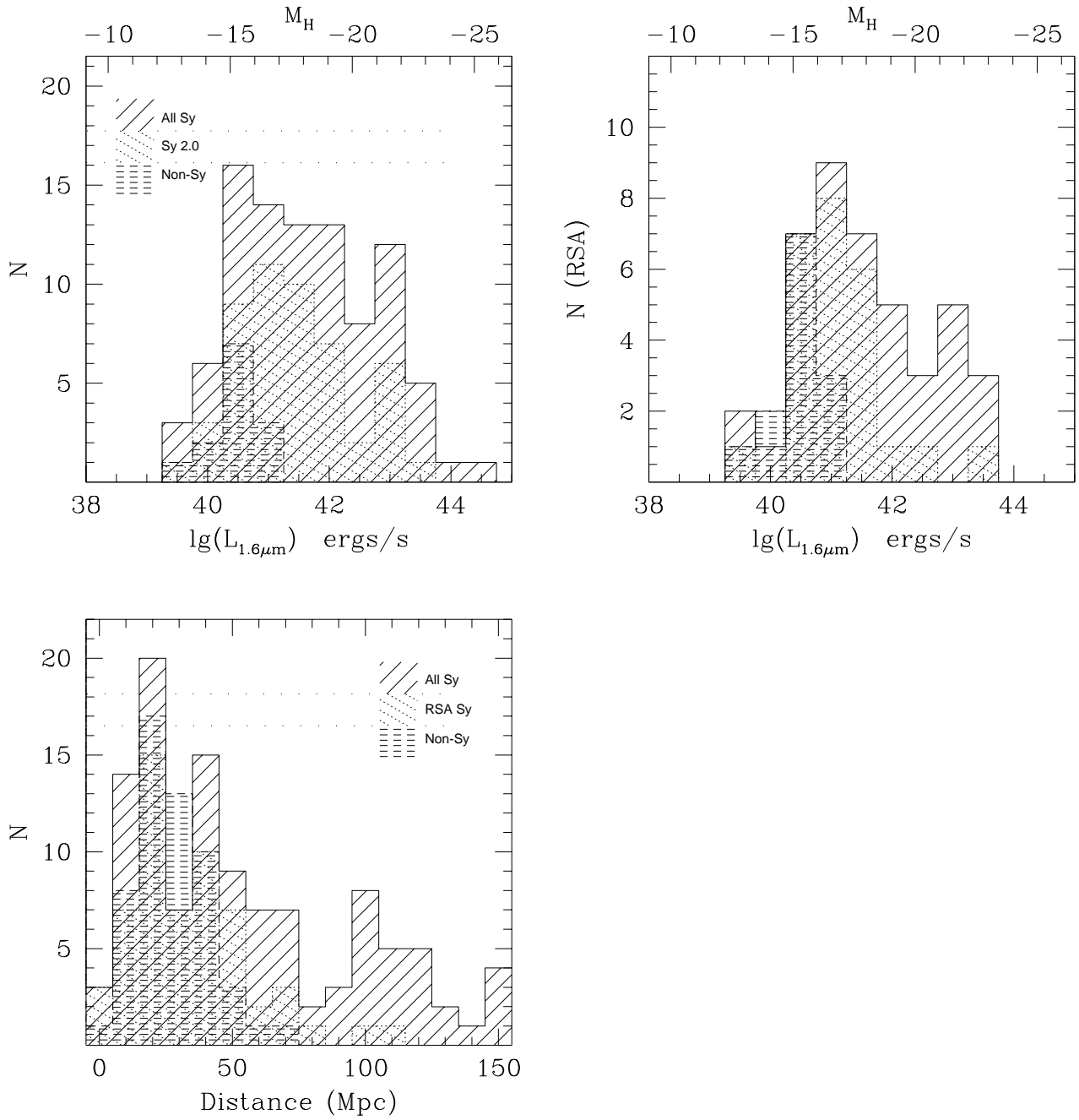


Fig. 2.— a) Luminosity distribution for the Seyferts with unresolved sources. The histogram filled with solid lines shows all the Seyferts listed in Tables 1-3, and the histogram filled with dotted lines corresponds to the Seyfert 2.0 galaxies. The histogram filled with dashed horizontal lines corresponds to the unresolved sources in the non-Seyfert, control galaxies. Absolute H magnitudes are shown on the top of the histograms. b) Luminosity distribution for the Seyferts in the RSA sample. c) Distance distribution for the total Seyfert, the RSA Seyfert and non-Seyfert samples. The distance distribution of the non-Seyfert galaxies matches that of the RSA sample.

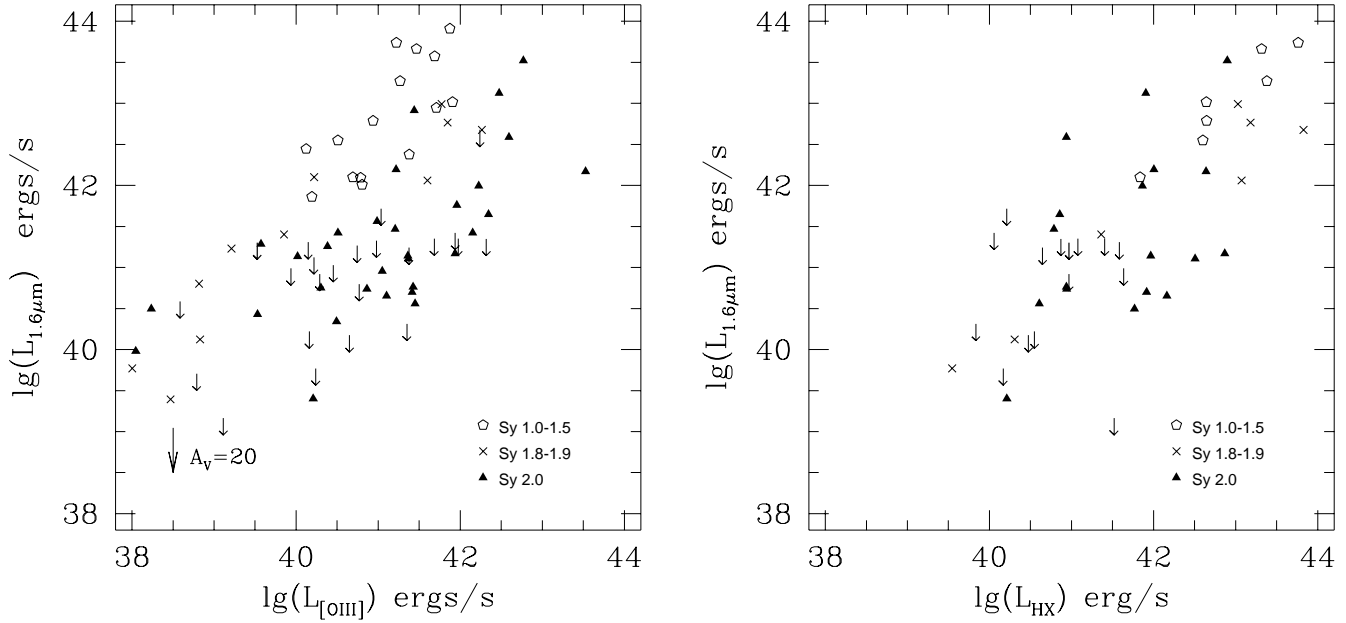


Fig. 3.— a) Correlation between $1.6\mu\text{m}$ and $[\text{OIII}]5007\text{\AA}$ luminosities for the Seyferts listed in Tables 1-3. Upper limits are given when no nuclear point source was detected at $1.6\mu\text{m}$. Seyfert 2.0 galaxies appear to have weaker $1.6\mu\text{m}$ luminosities compared to Seyfert 1.9-1.0 galaxies. The correlation between $[\text{OIII}]$ and $1.6\mu\text{m}$ luminosity suggests that the majority of the unresolved sources are non-stellar. $[\text{OIII}]5007\text{\AA}$ fluxes were taken from Ho et al. (1995), Whittle (1992), Bassani et al. (1999) and Risaliti et al. (1999) and whenever possible are corrected for reddening using the Balmer decrement. Points or upper limits are shown only when we found $[\text{OIII}]$ fluxes in these compilations. b) Correlation between $1.6\mu\text{m}$ and hard X-ray luminosities. Hard X-ray fluxes (2-10keV) were taken from Bassani et al. (1999), Risaliti et al. (2000) and Mulchaey et al. (1994) and were corrected for observed absorption, though some of the Seyfert 2.0 galaxies are Compton thick and so the fluxes do not represent the true X-ray luminosities. Points or upper limits are shown only when we found hard X-ray fluxes in these studies.

Table 1. RSA Seyfert Sample

Galaxy	Nucleus	Type	Proposid	v_{hel} km/s	profile	f_{nuc} mJy	$S_0 S_{r=1''}$ mJy $''^{-2}$	$h \alpha$
(1)	(2)	(3)	(4)	(5)	(6)	(7)	(8)	(9)
NGC 788	-	2	7330/2	4078	P	< 0.2	1.34	0.97
NGC 1068 ^{c,h}	*	2/1.8	7215/2	1137	-	83.6 ± 8	-	-
NGC 1241	:	2	7330/2	4052	P	0.17 ± 0.07	2.49	0.41
NGC 1275 ^h	*	1.9/1.5	7330/2	5264	-	4.30 ± 0.43	-	-
NGC 1320	*	2	7330/2	2716	P	1.15 ± 0.35	2.67	0.74
NGC 1386	-	2	7458/2	868	P	< 0.2	7.84	0.41
NGC 1667 ^h	-	2	7330/2	4547	P	< 0.3	1.56	0.79
NGC 2273 ^h	:	2	7172/2	1849	P	0.32 ± 0.28	3.50	0.61
NGC 2639 ^h	-	2/1.9	7330/2	3187	E	< 0.15	21.82	0.32
NGC 3031 ^h	*	1.8/1.5	7331/2	-34	-	13.4 ± 1.3	-	-
NGC 3081	:	2	7330/2	2385	P	0.22 ± 0.13	1.96	0.67
NGC 3227 ^{c,h}	*	1.5	7172/2	1157	-	13.2 ± 1.3	-	-
NGC 3362 ^c	F	2	7867/1	8318	P	0.05 ± 0.02	0.32	0.84
NGC 3393	-	2	7330/2	3750	P	< 0.25	2.38	0.73
NGC 3516 ^{c,h}	*	1.2	7330/2	2649	-	18.1 ± 1.8	-	-
NGC 3786 ^c	*	1.8	7867/1	2678	E	3.25 ± 0.33	18.97	0.33
NGC 3982 ^{c,h}	F	2/1.9	7330/2	1109	P	0.34 ± 0.11	1.29	0.65
NGC 4151 ^{c,h}	*	1.5	7215/2	995	-	112.1 ± 11	-	-
NGC 4235 ^{c,h}	*	1.2	7328/2	2410	P	3.69 ± 0.38	3.10	0.39
NGC 4253 ^c	*	1.5	7330/2	3876	-	20.0 ± 2.0	-	-
NGC 4258 ^h	-	2/1.9	7230/2	448	P	< 1.0	5.35	0.98
NGC 4388 ^{c,h}	*	2/1.9	7867/1	2524	P	0.71 ± 0.22	1.61	0.80
NGC 4395 ^{c,h}	*	1.8	7330/2	319	-	0.85 ± 0.18	-	-
NGC 4593	*	1	7330/2	2698	-	10.1 ± 1.0	-	-
NGC 4594 ^h	-	1.9/L2	7331/2	1091	P	< 1.4	30.28	0.38
NGC 4785	-	2	7330/2	3735	P	< 0.3	2.79	0.70
NGC 4939	F	2	7330/2	3111	P	0.36 ± 0.06	1.89	0.47
NGC 4941	-	2	7330/2	1108	P	< 0.4	3.10	0.71
NGC 4945	-	2	7865/2	560	E	< 0.15	21.27	0.41
NGC 5005 ^h	-	2/L1.9	7330/2	946	P	< 3.2	8.88	0.82
NGC 5033 ^{c,h}	*	1.9/1.5	7330/2	875	P	3.22 ± 0.46	4.97	0.64

Table 1—Continued

Galaxy	Nucleus	Type	Proposid	v_{hel} km/s	profile	f_{nuc} mJy	$S_0 S_{r=1''}$ mJy $''^{-2}$	$h \alpha$
(1)	(2)	(3)	(4)	(5)	(6)	(7)	(8)	(9)
NGC 5128	*	2	7330/2	547	-	5.8 ± 0.6	-	-
NGC 5135	*	2	7330/2	4112	P	0.66 ± 0.07	1.57	0.50
NGC 5194 ^h	:	2	7327/2	463	E	0.19 ± 0.18	17.16	0.74
NGC 5273 ^{c,h}	*	1.9/1.5	7330/2	1089	P	1.67 ± 0.17	2.18	0.45
NGC 5347 ^c	*	2	7330/2	2335	P	0.97 ± 0.24	1.20	0.85
NGC 5427	*	2	7330/2	2618	P	0.42 ± 0.09	0.59	0.78
NGC 5506	*	1.9	7330/2	1853	-	53.1 ± 5.3	-	-
NGC 5548 ^{c,h}	*	1.2/1.5	7172/2	5149	P	17.7 ± 1.8	1.18	0.50
NGC 5643	-	2	7330/2	1199	P	< 1.7	2.60	1.09
NGC 5674 ^c	*	1.9	7867/1	7474	E	2.62 ± 0.26	12.01	0.30
NGC 5953	F	2	7330/2	1965	P	0.37 ± 0.26	4.36	0.56
NGC 6221	*	2	7330/2	1482	P	3.14 ± 0.30	3.48	0.32
NGC 6300	*	2	7330/2	1110	P	1.97 ± 0.20	3.01	0.37
NGC 6814	*	1.5	7330/2	1563	P	6.25 ± 0.63	3.04	0.44
NGC 6890	*	2	7330/2	2419	E	0.80 ± 0.09	5.14	0.76
NGC 7130	-	2	7330/2	4842	E	< 0.15	17.22	0.32
NGC 7469 ^c	*	1.2	7219/2	4892	-	48.3 ± 4.8	-	-
NGC 7479 ^h	:	2/1.9	7331/2	2381	P	0.24 ± 0.14	1.63	0.71
NGC 7496	-	2	7330/2	1649	P	< 1.4	0.63	1.36
NGC 7582	*	2	7330/2	1575	P	22.6 ± 2.3	5.08	0.31
NGC 7743 ^h	-	2	7330/2	1710	P	< 0.5	2.57	1.13
IC 2560	:	2	7330/2	2925	P	0.16 ± 0.09	2.99	0.42
IC 5063	*	2	7330/2	3402	P	0.32 ± 0.12	2.42	0.63
CIRCINUS	*	2	7273/2	436	P	4.77 ± 0.7	12.74	0.51
MRK 1066	F	2	7330/2	3605	P	0.51 ± 0.16	3.53	0.60
IRAS1832-5926	*	2	7328/1	6065	-	22.7 ± 4.0	-	-

Table 1—Continued

Galaxy	Nucleus	Type	Proposid	v_{hel}	profile	f_{nuc}	$S_0 S_{r=1''}$	$h \alpha$
(1)	(2)	(3)	(4)	km/s	(6)	mJy	mJy $''^{-2}$	(9)

^cThis galaxy is also part of the CfA Seyfert sample (Huchra & Burg 1992; Osterbrock & Martel 1993)

^hThis galaxy is also part of the sample studied by Ho, Filippenko & Sargent (1995).

Note. — This table contains galaxies which were part of the RSA Seyfert sample listed by Maiolino & Rieke (1995). Columns (1) Galaxy; (2) Type of nucleus seen in the F160W (1.6 micron) NICMOS images. When the nucleus displayed a clear diffraction ring we denote ‘*’, when the ring was extremely faint we denote ‘F’, and when the galaxy was resolved we denote ‘.’. When there was an unresolved peak but no sign of a diffraction ring we denote ‘:’. (3) Seyfert type. These classifications are following those compiled from the literature by Maiolino & Rieke (1995), and listed in Osterbrock & Martel (1993) or Ho et al. (1995). When classifications differed we listed the classification on the left by Maiolino & Rieke followed by that of Ho et al. on the right; (4) Heliocentric velocity in km/s; (5) HST Proposal ID for the 1.6 micron images followed by the NICMOS camera number used to image the galaxy; (6) Best fitting surface brightness profile shape in the central arcsecond. We fit the sum of an unresolved nuclear source and either an exponential profile ($S(r) = S_0 e^{-r/h}$) or a powerlaw profile ($S(r) = S_{r=1''} r^{-\alpha}$). P refers to the powerlaw and E refers to the exponential. When an unresolved nuclear component dominates the central arcsecond we do not record the profile shape. (6) The flux of the unresolved component in mJy. Errors are estimated based on the difference between nuclear fluxes estimated from the best unresolved+exponential profile fit and that of the best unresolved+powerlaw profile fit. We restricted the estimated error to be larger than 10% of the unresolved component estimated from the best fit. When the galaxy was resolved we list as an upper limit the flux of an unresolved component which was the result of the best fitting unresolved+exponential profile fit. (7) When the galaxian profile fit was an exponential we record the central surface brightness S_0 , in mJy/arcsecond². When the galaxian profile shape was a power law we record the surface brightness, $S_{r=1''}$, at a radius of 1''. (8) When the galaxian profile fit was an exponential we record exponential scale length, h , of the galaxian component in arcseconds. When the galaxian profile fit was a powerlaw we record the exponent α . When the point source was extremely bright, the galaxian profile was not constrained so S and h or α are not listed.

Table 2. Additional Seyferts which are in the CfA sample

Galaxy	Nucleus	Type	Proposid	v_{hel} km/s	profile	f_{nuc} mJy	$S_0 S_{r=1''}$ mJy $''^{-2}$	$h \alpha$
(1)	(2)	(3)	(4)	(5)	(6)	(7)	(8)	(9)
NGC 1144	:	2	7867/1	8648	E	0.08 ± 0.08	8.56	0.38
NGC 5252	F	1.9	7330/2	6926	P	0.60 ± 0.21	1.34	0.80
NGC 5283	-	2	7867/1	2700	P	< 0.3	1.99	0.91
NGC 5695	-	2	7867/1	4225	P	< 0.2	1.65	0.72
NGC 5929	-	2	7330/2	2492	P	< 0.25	1.64	0.81
NGC 5940	*	1	7328/1	10115	E	0.93 ± 0.21	4.21	0.34
NGC 6104	*	1.5	7328/1	8382	P	0.13 ± 0.05	0.45	0.75
NGC 7674	*	2	7328/1	8713	E	4.39 ± 0.44	13.57	0.22
NGC 7682	-	2	7867/1	5134	P	< 0.01	0.75	0.77
MRK 231	*	1	7213/2	12642	-	80.1 ± 8.0	-	-
MRK 266	-	2	7328/2	8360	P	< 0.1	1.85	0.48
MRK 334	*	1.8	7867/1	6582	E	6.83 ± 0.86	60.62	0.11
MRK 461	-	2	7867/1	4856	P	< 0.4	0.63	1.21
MRK 471	*	1.8	7328/1	10263	E	0.32 ± 0.04	3.54	0.52
MRK 573	F	2	7330/2	5174	P	0.54 ± 0.23	1.90	0.73
UGC 6100	-	2	7867/1	8778	P	< 0.15	0.87	0.92
UGC 12138	*	1.8	7328/1	7375	E	2.59 ± 0.26	10.50	0.37
UM 146	*	1.9	7328/1	5208	E	0.82 ± 0.19	5.64	0.29

Note. — See Table 1 for more information.

Table 3. Additional Seyferts

Galaxy	Nucleus	Type	Proposid	v_{hel} km/s	profile	f_{nuc} mJy	$S_0 S_{r=1''}$ mJy $''^{-2}$	$h \alpha$
(1)	(2)	(3)	(4)	(5)	(6)	(7)	(8)	(9)
NGC 1672	-	2	7330/2	1350	P	< 1.1	4.80	0.83
NGC 3079 ^h	-	2	7330/2	1125	P	< 0.1	7.43	0.24
NGC 3486 ^h	F	2	7330/2	681	P	0.78 ± 0.31	1.68	0.83
NGC 3718 ^h	:	L1.9	7330/2	994	P	0.98 ± 0.61	4.89	0.73
NGC 4117	F	2	7330/2	958	P	0.24 ± 0.18	1.07	0.81
NGC 4303 ^h	*	2/H	7330/2	1566	P	3.72 ± 0.37	3.84	0.58
NGC 4725 ^h	-	2	7330/2	1206	P	< 0.7	4.60	0.79
NGC 4968	-	2	7330/2	2957	P	< 0.4	1.33	1.08
NGC 6951 ^h	-	2	7330/2	1424	P	< 0.3	2.55	0.80
MRK 1210	*	2	7330/2	4046	E	1.51 ± 0.15	6.47	0.41
MRK 78	-	2	7330/2	11137	P	< 0.6	1.44	1.07
MRK 477	F	2	7330/2	11332	P	0.29 ± 0.16	0.31	1.10
ESO138-G1	*	2	7330/2	2740	P	5.36 ± 0.67	1.89	0.23
ESO137-G34	-	2	7330/2	2747	P	< 0.1	1.44	1.07
ESO362-G08	-	2	7328/1	4785	P	< 0.3	4.32	0.70
IRAS1443+2714	*	2	7328/1	8814	E	1.96 ± 0.20	5.57	0.28
IRAS2302-0004	*	2	7328/2	7585	E	3.82 ± 0.38	7.89	0.23
IRAS1833-6528	-	2	7328/2	3983	P	< 0.3	1.95	0.87
NGC 1019	*	1	7328/1	7251	E	1.27 ± 0.16	7.29	0.27
NGC 7319	:	2	7328/2	6764	P	0.07 ± 0.02	0.68	0.73
MRK 1	-	2	7328/1	4780	P	< 0.2	0.40	1.23
MRK 6	*	1.5	7328/1	5537	E	30.6 ± 3.1	9.29	0.23
MRK 40	*	1	7328/1	6323	E	0.78 ± 0.18	6.59	0.27
MRK 42	*	1	7328/1	7200	E	1.35 ± 0.25	4.56	0.23
MRK 176	*	2	7328/2	8346	E	2.96 ± 0.30	16.34	0.31
MRK 372	*	1.5	7328/1	9300	E	0.69 ± 0.10	14.51	0.27
MRK 493	*	1	7328/1	9569	P	4.74 ± 0.47	0.23	1.23
MRK 516	:	1.8	7328/1	8519	E	0.18 ± 0.10	15.82	0.22
MRK 915	*	1	7328/1	7228	P	4.25 ± 0.43	0.59	0.97
MRK 1048	*	1	7328/2	12934	P	12.2 ± 1.2	0.39	1.05
MRK 1261	F	1	7328/1	7808	P	0.18 ± 0.02	1.31	0.69

Table 3—Continued

Galaxy	Nucleus	Type	Proposid	v_{hel} km/s	profile	f_{nuc} mJy	$S_0 S_{r=1''}$ mJy $''^{-2}$	$h \alpha$
(1)	(2)	(3)	(4)	(5)	(6)	(7)	(8)	(9)
MRK 1308	*	2	7328/2	1087	E	0.89 ± 0.21	1.18	0.62
IC 4870	*	2	7328/2	889	E	0.62 ± 0.17	2.14	0.15
UM 625	*	2	7328/1	7495	E	0.23 ± 0.03	2.42	0.60
NGC 4472 ^h	-	2	7453/2	868	P	< 0.05	0.04	~ 0.0
NGC 4565 ^h	F	1.9	7331/2	1282	P	0.63 ± 0.24	6.55	0.44
IC 4329A	*	1.2	7172/2	4813	-	59.4 ± 5.9	-	-

Note. — This table lists additional Seyferts from proposals 7330, 7328, from the tabulation of Ho et al. (1995) and the Seyfert 1 galaxy IC 4329A. See Table 1 for more information.

Table 4. Control galaxies with unresolved nuclear sources

Galaxy	Nucleus	Type	Proposid	v_{hel} km/s	profile	f_{nuc} mJy	$S_0 S_{r=1''}$ mJy $''^{-2}$	$h \alpha$
(1)	(2)	(3)	(4)	(5)	(6)	(7)	(8)	(9)
NGC 157	F		7330	1668	P	0.29 ± 0.08	1.75	0.24
NGC 404	*	L2	7330	-48	P	2.99 ± 1.81	1.76	1.19
NGC 578	*		7330	1630	E	0.24 ± 0.02	0.71	1.42
NGC 864	:	H	7330	1562	P	0.31 ± 0.06	0.72	0.59
NGC 1530	F		7330	2461	P	0.25 ± 0.02	1.67	0.24
NGC 2776	F	H	7330	2626	P	0.16 ± 0.03	0.68	0.53
NGC 4030	F		7330	1460	P	0.43 ± 0.11	2.00	0.53
NGC 4380	F	H	7330	967	P	0.13 ± 0.08	0.56	0.78
NGC 5383	:	H	7330	2250	P	0.07 ± 0.04	1.24	0.43
NGC 5970	F	L2	7330	1957	E	0.09 ± 0.01	1.73	1.58
NGC 6384	:	T2	7330	1665	P	0.17 ± 0.05	1.96	0.38
NGC 6412	:	H	7330	1324	P	0.09 ± 0.01	0.27	0.26
NGC 7126	:		7330	2981	E	0.22 ± 0.10	5.60	0.47

Note. — See Table 1 for more information. All these images were observed with Camera 2. When possible, classifications from Ho et al. (1995) are shown.

Table 5. Control galaxies lacking unresolved emission

Galaxy	v_{hel}	Profile	$S_0 S_{r=1''}$	$h \alpha$
NGC 214	4534	P	1.09	0.75
NGC 357	2406	P	2.70	0.66
NGC 628	657	P	0.20	1.28
NGC 1300	1568	P	1.52	0.96
NGC 1398	1407	P	6.63	0.64
NGC 1638	3320	P	2.82	0.60
NGC 1961	3934	P	2.55	0.54
NGC 2179	2798	E	9.01	0.68
NGC 2223	2722	P	9.01	0.68
NGC 2336	2204	P	1.55	0.69
NGC 2460	1442	P	1.91	0.84
NGC 2841	638	P	8.95	0.63
NGC 2903	556	P	1.63	0.92
NGC 2985	1322	P	3.39	0.84
NGC 3032	1533	P	1.19	1.52
NGC 3145	3506	P	2.73	0.52
NGC 3300	3045	P	1.27	0.78
NGC 3351	778	P	2.65	0.39
NGC 3368	897	P	5.95	0.83
NGC 3458	1818	P	3.67	0.74
NGC 3627	897	P	5.88	0.78
NGC 3630	727	P	4.92	0.75
NGC 3865	1509	E	10.07	0.32
NGC 4143	985	P	6.74	0.70
NGC 4254	2407	P	0.69	1.15
NGC 4260	1958	P	1.44	0.67
NGC 4314	963	P	2.75	0.67
NGC 5054	1741	P	2.11	0.88
NGC 5064	3002	P	4.45	0.55
NGC 5614	3892	P	3.64	0.79
NGC 5691	1870	P	0.21	0.54
NGC 5739	5377	P	4.31	0.69
NGC 6744	841	P	2.69	0.77

Table 5—Continued

Galaxy	v_{hel}	Profile	$S_0 S_{r=1''}$	$h \alpha$
NGC 6946	48	E	21.55	0.86
NGC 7096	3100	E	12.06	0.56
NGC 7177	1150	E	8.81	0.84
NGC 7392	3192	P	1.90	0.86
NGC 7716	2571	P	2.29	0.74
NGC 7744	3098	P	4.66	0.80
NGC 7814	1050	E	10.91	0.94
IC 5267	1713	P	3.70	0.76

Note. — All galaxies were part of proposal 7330 and were observed with NICMOS Camera 2. See Table 1 for more information.

Table 6: Numbers of Seyfert Galaxies with point sources

Sample	2.0					1.8-1.9				1.0-1.5		Total Sy	Non-Sy				
	*	F	:	-	%Res	*	F	:	-	*	F		*	F	:	-	%Res
CfA	4	3	1	7	53 47	9	1	0	0	10	0	35					
RSA	14	5	6	14	64 49	8	0	0	1	9	0	57					
7330	13	8	3	19	56 49	5	1	1	0	4	0	54	2	6	5	41	24 15
Ho	0	1	2	6	33 11	3	2	1	2	9	0	26					
All Sy	24	9	8	32	56 45	12	2	2	1	21	1	112					

Note. — The types of nuclei seen (*, F, :, -) are described in the caption to Table 1. We list here the number of each type of Seyfert galaxy with each type of nucleus. For the Seyfert 2 and non-Seyfert samples we also list in the column labelled %Res the percent of Seyferts of that type with emission from an unresolved component (type *, F or :) and that from an unresolved component at high confidence (type * and F). The subsets considered here are the Seyfert galaxies which are part of the CfA and RSA samples, galaxies from HST proposal 7330 including Seyfert and non-Seyfert samples, Seyferts which were also tabulated by Ho et al. (1995), and all the Seyferts we have listed in Tables 1-3. We have used classifications listed in Maiolino & Rieke (1995) except for the Ho et al. sample in which case we use their classifications. All Seyfert 1.0-1.5 galaxies listed Tables 1-3 display prominent unresolved nuclear sources. Almost all Seyfert 1.8 or 1.9 galaxies display some level of unresolved emission. About 50% of the Seyfert 2 galaxies display significant unresolved emission compared to $\sim 25\%$ of the normal galaxies from proposal 7330. Proposal 7330 contains a non-Seyfert sample with distribution that is intended to match that of its Seyfert sample.

Table 7. Correlation Statistics

Type	Quantities	N	R_s	Probability
Sy1.0-1.9	[OIII] vs. $1.6\mu\text{m}$	26	0.67	> 0.99
Sy2.0	[OIII] vs. $1.6\mu\text{m}$	31	0.22	0.75
Sy1.0-1.9	HX vs. $1.6\mu\text{m}$	14	0.78	> 0.99
Sy2.0	HX vs. $1.6\mu\text{m}$	18	0.34	0.83

Note. — Spearman rank-order correlation coefficient, R_s for Seyferts shown in Figure 3. The probability of a correlation between fluxes (not luminosities) are shown in the right most column. The number of objects is given by N .